Model for the Evolving Bed Surface around an Offshore Monopile

Hartvig, Peres Akrawi

Published in:
Coastal Engineering Journal

Publication date:
2012

Document Version
Early version, also known as pre-print

Model for the Evolving Bed Surface around an Offshore Monopile

Peres Akrawi Hartvig

Department of Civil Engineering, Aalborg University, Niels Bohrs Vej 8, 6700 Esbjerg, Denmark

Abstract

This paper presents a model for the bed surface around an offshore monopile. The model has been designed from measured laboratory bed surfaces and is shown to reproduce these satisfactorily for both scouring and backfilling. The local rate of the bed elevation is assumed to satisfy a certain general parametrized surface. The model also accounts for sliding of sediment particles when the angle of the local bed slope exceeds the angle of repose.

Keywords: Bed surface, seabed, erosion, scour, backfilling, time variation, temporal, sliding, monopile, Exner equation, predictor, corrector

1. Introduction

The scour of the bed surface around an offshore monopile is known to emerge from the play between the sediment and the fluid. The sediment responds to the fluid e.g. by being entrained from the bed into suspension and convected away, rolling or sliding along the bed or being deposited from suspension into the bed. The fluid responds to the sediment, e.g. by changing its bulk viscosity due to suspended grains or dislocating and resizing its vortices due to a scoured bed surface.

The monopile finds itself in the midst of this fascinating multiphase play, comprised of the three actors: water, air and bed material. From a designer's perspective, the development of the *bed surface* is of significant importance since it has a strong impact on the structural performance of the monopile and its superstructure. The bed surface evolves perpetually in the most general case, typically being plane before installation of the foundation, undergoing scouring at the time of the installation and onwards and perhaps also experiencing intermittent situations where the hole has been backfilled by ocean waves with or without current due to weakened

flow conditions. In lieu of knowledge of the bed surface, knowledge of the approximate *depth*, *volume* and *shape* of the hole may be sufficient quantities for designing the foundation.

To furnish the prediction of either the bed surface or the depth, volume and shape, it is necessary to handle the sediment-fluid play in a tractable way. In light of its inherent complexity, it seems fruitful at this stage to reduce the degrees of freedom in the physical problem. Since the bed elevation h is wanted for design and is also central to the physical problem, I have dealt with its local rate (of change per unit time), $\partial h/\partial t$, that can be integrated with respect to time to yield the bed elevation h.

In this paper, I propose modeling the main contribution of the bed elevation rate by a certain parametrized surface that caters both for scouring and backfilling. This is the main novelty of this study and is encapsulated in what I call the *predictor* component of the present model. I also propose a *corrector* component that accounts for sliding of the sediment particles when the angle of the local bed slope exceeds the angle of repose – a correction that is shown to be crucial for scouring. Many aspects of the corrector have been been inspired by Roulund et al. (2005), Roulund (2000) and Umeda et al. (2006) but my contribution lies in clarifying the formulation and comparing its performance with the experiments that I have recently published in Hartvig et al. (2010). Finally, the present study details how the bed elevation rate is related to the rates of the scour depth and scour volume that I have previously presented in Hartvig et al. (2010).

I foresee at least two potential applications of the model:

1. Given time series of scour depth and scour volume, the model can be used to forecast the development of the bed surface. This information can then enter as input for analyses of the soil, the foundation and its superstructure as well as for design decisions.
2. The model provides a basis for linking the development of the scour depth and volume to the development of the bed shear stress. This requires the additional use of the Exner equation, as given below, to link the local rate of the bed elevation and the bed flux and the use of a sediment transport formula to link the bed flux and the bed shear stress. This chain of links can contribute to bridging an epistemological deficit in either of the linked items. As an example for a given flow condition, the model allows one to estimate the development and distribution of the bed shear stress based on the development of the scour depth and volume – or vice versa.

In connection with the first point, the present paper demonstrates this application but I must admit that it focuses on *hindcasting* a limited set of measured laboratory bed surfaces. Validation against a larger set of experiments is encouraged but may not fully redeem a poor *forecasting* performance where the model input parameters are expected to be less accurately determined.

To clarify the second point and to allow for later references when I detail the local sliding procedure, I would like to introduce the Exner equation already here. If the sediment can be decomposed into a *suspended* and *bed* load and the latter can be regarded as an incompressible continuum, then the conservation of mass or volume of the bed material is expressed by the Exner partial differential equation. It is written here with index notation and summation over terms with repeated tensor indices as:

$$(\kappa - 1) \cdot \frac{\partial h}{\partial t} = \frac{\partial Q_\alpha}{\partial x_\alpha} + \text{sink terms}, \quad t > 0 \tag{1.1}$$

In the equation, κ is the porosity in the range $[0, 1[$, h is the bed elevation defined positive upwards from a reference level, $\alpha = 1, 2$ is the tensor index with $x_\alpha = (x_1, x_2) \equiv (x, y)$, Q_α is the volumetric flux of the bed load per unit width and $\partial Q_\alpha / \partial x_\alpha \equiv \partial Q_x / \partial x + \partial Q_y / \partial y$ is the divergence of the volumetric flux. The quantities κ, h, Q_α and the sink terms are generally functions of the two-dimensional spatial plane x, y and time t. The equation provides a link between the bed elevation, the volumetric bed flux and the transfer between suspended and bed load at each bed point by the sink terms. In loose words, the above equation states that for an infinitesimal control curve enclosing each point, the local erosion – when corrected for porosity – is equal to the rate of volume per unit area flowing out as bed load and by other means. The bed flux is known to be a function of the sediment and flow conditions and appears in conventional time-averaged bed load formulas. It is the local rate of the bed elevation $\partial h / \partial t$ that I propose to model and its parameters may provide insight into the nature of the remaining quantities in (1.1) when investigating scouring or backfilling around offshore monopiles.

The rest of the paper is organized in three lumps: In Sec. 2, I present the theoretical and experimental background for the model. In Secs. 3-5, I present the mathematical formulation of the particular elements of the model. Finally, in Secs. 6-7, I compare the performance of model-based simulations relative to the experiments and discuss and conclude on these.

2. Background

The present study builds on the theoretical concepts and experimental results that I have previously presented in Hartvig et al. (2010) and will recap here. The paper of Hartvig et al. (2010) presented experiments of a model-scale monopile that had undergone scouring or backfilling in response to alternating flow conditions in laboratory flumes, conducted by a fellow co-author. At several instances in time during the experiments, the flow generation was temporarily paused and the upper-piece of the pile temporarily dismantled to allow a movable laser device to measure the bed surface in the vicinity of the pile.

2.1. Scour geometry parameters

In this section, I will present the scour geometry parameters used in the Hartvig et al. (2010) paper that I also adopt here and are crucial to the present method. Some comments on the parameters is presented here but a comprehensive description and discussion is beyond the scope of this paper.

The scour depth is a conventional but ambiguous parameter used in existing research. Aside from errors due to the discretization of the bed grid and technical errors in the measurements nearest the pile base, I essentially defined the scour depth S as the average depth of the bed along the pile base at a given moment in time. In mathematical terms and polar coordinates, this can be expressed as:

$$S(t) = -\frac{1}{2\pi} \int_{-\pi}^{\pi} h(r = r_{\min}, \theta, t)\, d\theta \tag{2.1}$$

where $r \geq 0$ is the radius from the pile axis and $\theta \in [-\pi; \pi]$ is the counterclockwise angle relative to the streamwise direction x. The pile base is thus defined as the closed curve fulfilling $r = r_{\min}$. For example, a circular pile with outer diameter D yields a circular boundary with $r_{\min} = D/2$. The negative sign accounts for the opposite definition of positive directions of h and S.

I have only come across one use of the volume of the scour hole in others' work, namely Link and Zanke (2004). In the present framework, the scour volume V plays a central role and is conceptually defined as the volume of void in the domain between the pile base and the outer boundary of the scour hole. Aside from the admitted difficulty of asserting the exact location of this latter outer boundary – a difficulty that increases for

smaller holes – and the discretization error, the scour volume can be expressed mathematically as:

$$V(t) = -\int_{\theta=-\pi}^{\theta=\pi}\int_{r=r_{\min}}^{r=r_{\max}} h(r,\theta,t)\; r\; dr\; d\theta \tag{2.2}$$

The outer boundary of the scour hole is defined by the closed curve fulfilling $r = r_{\max}$ and the domain enclosed by the pile base and the outer boundary is termed the *scour domain* Ω. These are illustrated in Fig. 4.2 for the circular-elliptic scour domain used in the present paper and differs slightly from the purely elliptic domain in Hartvig et al. (2010). The negative sign again accounts for the different sign conventions.

Based on these two quantities, the scour volume and scour depth, I introduced a parameter, coupling them together. The scour shape factor ψ, as I call it, was implicitly defined by the following identity:

$$V = \psi S^3 \tag{2.3}$$

Finally, I want to clarify my notion of *scour*. I did not offer this clarification in Hartvig et al. (2010) but now it appears more pertinent. To honor the conventional sense of *scour*, I still use this term broadly for erosion as well as deposition of sediment around offshore structures. When I refer to a more narrow sense of scour, namely the erosive action when viewed in contrast to depositing action and when such a distinction is possible, I call it *scouring*. In this way, *scour* and *scouring* become two subtly distinct notions and *scour* encompasses both *scouring* and *backfilling*. For a mathematical definition of the two latter terms in my framework, I use the scour volume rate rather than the scour depth rate to distinguish among them by the following criterion:

$$\begin{aligned} \text{Scouring:} \quad & dV/dt > 0 \\ \text{Backfilling:} \quad & dV/dt < 0 \end{aligned}$$

2.2. *Parameter development*

Having now presented the key scour geometry parameters, I will proceed to describe their development. In Hartvig et al. (2010), I proposed a particular set of ordinary differential equations, which I will refer to as *development equations*, for modeling the temporal development of V and S. These equations are provided here in order to deliver the scour volume rate and scour depth rate at each time step that is required as input by the current flow of computations.

In this connection, I would like to make three brief comments. First, the present model is not restricted to the use of these particular versions of the development equations. Other equations or interpolation from tables could be adopted to deliver the needed rates for the model in the current computational flow. Secondly, the development equations and the values of their parameters were inferred from a limited set of test conditions. They have not been validated by other studies or researchers at similar or more general test conditions. For hindcasting purposes, they appear adequate but this is not necessarily true for forecasting as noted before. Finally, the parameters of the development equations are introduced below but their values are given Sec. 6. The present values differ somewhat from those that I reported in Hartvig et al. (2010) because I there inadvertedly over-predicted the values of the scour volume due to a systematic calculation error and this error has propagated into the values of the parameters of the development equations. The values that are used here are the correct ones. (Note to reviewers: I expect to issue an errata to the 2010 paper, so this last remark may not be necessary in the final manuscript.)

Aside for some systematic deviation for smaller backfilled holes, I found that the scour volume rate during both scouring and backfilling approximately satisfies the following linear differential equation:

$$\frac{dV}{dt} = \frac{V_\infty - V}{t_V}, \quad t > 0 \tag{2.4a}$$

which has the solution:

$$V = V_\infty + (V_0 - V_\infty)\, e^{-t/t_V} \tag{2.4b}$$

where V_0, V_∞ and $t_V > 0$ are fitting parameters that are constant with respect to time and interpreted as the scour volume of the initial bed, the scour volume of the equilibrium bed and a characteristic time for the scour volume development, respectively.

The development of the scour shape factor appeared to depend on whether the sedimentation regime was scouring or backfilling. For *scouring*, it was difficult to achieve a generally valid fit but for the present purpose, the following differential equation can be used:

$$\frac{d\psi}{dt} = \frac{\psi_\infty - \psi}{t_\psi}, \quad t > 0 \tag{2.5a}$$

which has the solution:

$$\psi = \psi_\infty + (\psi_0 - \psi_\infty)\, e^{-t/t_\psi} \tag{2.5b}$$

where ψ_0, ψ_∞ and $t_\psi > 0$ are fitting parameters that are constant with respect to time and are interpreted as the scour shape factor of the initial bed, the scour shape factor of the equilibrium scoured bed and a characteristic time for the scour shape factor development, respectively.

For *backfilling*, the following differential equation was approximately satisfied:

$$\frac{d\psi}{d(V/D^3)} = -c_1 \cdot \left(\frac{V}{D^3}\right)^{-c_2} \tag{2.6a}$$

which has the solution:

$$\psi = \psi_0 + \frac{c_1}{c_2 - 1} \cdot \left(\left(\frac{V}{D^3}\right)^{1-c_2} - \left(\frac{V_0}{D^3}\right)^{1-c_2}\right), \quad c_2 \neq 1 \tag{2.6b}$$

where ψ_0, c_1 and c_2 are dimensionless fitting parameters that are constant with respect to time and ψ_0 is again interpreted as the scour shape factor for the initial bed.

Having presented the above development equations, I can now clarify that I have not provided a direct equation for the development of the scour depth here. Instead, S or its rate dS/dt is determined indirectly by the use of both Eqs. (2.3) and (2.4) together with either (2.5) for scouring or (2.6) for backfilling.

2.3. Scour geometry features

The experimental bed profiles of Hartvig et al. (2010) provide the benchmark reference for the present model. The present model has evolved iteratively as new components were introduced or old ones changed and subsequent simulations were compared to the experimental data. To give an overview, I have outlined the features of the geometry of the scour hole during both scouring and backfilling that I have deemed important and that have guided my model design. Since the features appear to be general and physically plausible, it is worth emphasizing that they are based only on the limited test conditions of Hartvig et al. (2010) and are not confirmed by other studies according to my knowledge. An important exception, however, is the features of sliding during monopile scouring that have also been mentioned in Dey and Barbhuiya (2005), Roulund et al. (2005), Sumer and Fredsøe (2002, chap. 3.2) and Whitehouse (1998, chap. 7.2.1).

Before I proceed, I want to clarify my notion of the modifiers *upstream* or *downstream* when used before *scour domain* or *directions*. The lateral axis y is used to distinguish between the two regions of the *scour domain*, namely the

upstream scour domain with points fulfilling $(x < 0, y) \in \Omega$ and the *downstream* scour domain with points fulfilling $(x > 0, y) \in \Omega$. The *directions* are defined by Cartesian vectors placed in Origo $(x = 0, y = 0)$ where the *upstream* direction is determined by the vector $(-1, 0)$ and the *downstream* direction by the vector $(1, 0)$.

Now I am in the position to list the features of the scour geometry of which most can be examined with an eye to Figs. 6.1–6.6:

1. During scouring, the bed slope in the *upstream* scour domain – both in upstream and lateral directions – becomes and remains approximately linear. In contrast, the bed slope in the *downstream* scour domain is typically curved and less steep.
2. During backfilling, the bed slope in both the upstream and downstream scour domain become more curved. Furthermore, the extent of the outer boundary of the scour hole appears to remain constant although it may be expected to decrease if the hole becomes very small.
3. The radial extent of the *upstream* scour domain – both in upstream and lateral directions – is approximately constant with respect to the angle. In contrast, the radial extent of the scour domain in the *downstream* direction is typically different from and larger than that of the upstream scour domain.
4. The bed elevation varies along the base of the monopile. Often, the base bed elevation in the *upstream scour domain* – both in upstream and lateral directions – is approximately constant and lower than the base bed elevation in the *downstream direction*.
5. The bed elevation within the scour domain is approximately symmetrical about the longitudinal axis x.

Based on features 1, 3 and 4, the physical mechanism of sliding failure appears to be dominant during scouring in shaping the upstream scour domain and determining its extent. Based on feature 2, it appears that sliding plays a minor role during backfilling and that the sediment is deposited in the entire scour domain with the largest concentration near the pile. I will refer to these features as I present the different aspects of the model in the next sections.

3. Model overview

The present model follows is based on a rate approach that describes the local rate of the the bed elevation, $\partial h/\partial t$. Compared to describing the

bed elevation h itself, the differential approach based on the rates has the advantage of being more permissive and allowing a more complicated bed surface. Consequently, it mainly requires information on the *rates* of the scour volume and scour depth, dV/dt and dS/dt, at each time step, rather than the scour volume V and scour depth S themselves. This information is obtained from the development equation that I previously presented.

The model involves one or two components, namely the:

- predictor (mandatory)
- corrector (optional)

In one sense, the components convey a series of *steps* that are conducted at each time step. The predictor step dictates the main development of the bed elevation while the corrector step, when enabled by the user, may redistribute the bed elevation to account for sliding effects which appears to greatly improve scouring prediction. In this sense, the approach resembles that of conventional predictor-corrector schemes for solving ordinary differential equations and this resemblance has inspired my naming of the components.

In this connection, I want to emphasize that the predictor will account *indirectly* for *some* of the sliding effects when they are manifested in the development equations. For example, if sliding governs the geometry of the bed surface during scouring, the breadth of the hole will be governed by the depth, as detailed later. This property will be manifested in the development of dV/dt and dS/dt and will eventually be passed on to the predictor. On a minor note, the corrector step is actually placed *before* the predictor step in the current flow of computations as seen in Fig. 4.7.

In an equivalent sense, the components can be understood as *contributions* to the quantity in question. In the general case, the local rate of the bed elevation and the rates of the scour volume and scour depth can be decomposed into a predictor and corrector contribution, i.e.:

$$\frac{\partial h}{\partial t} = \left(\frac{\partial h}{\partial t}\right)_{\text{pre}} + \left(\frac{\partial h}{\partial t}\right)_{\text{cor}}, \quad t > 0 \tag{3.1a}$$

$$\frac{dV}{dt} = \left(\frac{dV}{dt}\right)_{\text{pre}} + \left(\frac{dV}{dt}\right)_{\text{cor}}, \quad t > 0 \tag{3.1b}$$

$$\frac{dS}{dt} = \left(\frac{dS}{dt}\right)_{\text{pre}} + \left(\frac{dS}{dt}\right)_{\text{cor}}, \quad t > 0 \tag{3.1c}$$

where the subscripts 'pre' and 'cor' denote *predictor* and *corrector*, respectively. This distinction is omitted in in-line formulas or text when it is irrelevant for the argument or when it is clearly provided by the context. The decomposition is relevant only when the corrector is enabled. When disabled, the corrector quantities are taken as nil, i.e. $(\partial h/\partial t)_{\text{cor}} = (dV/dt)_{\text{cor}} = (dS/dt)_{\text{cor}} = 0$.

The rates of scour depth and scour volume are decomposed into two contributions too because the corrector may indirectly change these through its redistribution of the bed elevation. The scour volume rate may change when sliding particles enter or leave the scour domain and the scour depth rate may change when the particles enter or leave the pile base. For example, when the bed elevation at the pile base is lifted due to a net inflow of sliding particles during a corrector step, we have $(dS/dt)_{\text{cor}} < 0$ at the current time step. The predictor must subsequently compensate for this deposition in order to maintain the given scour depth rate at the current time step. This idea should appear clearer from the following sections where the components and the flow diagrams are presented.

4. Predictor

The predictor is designed on the fundamental assumption that the local rate of the bed elevation, $(\partial h/\partial t)_{\text{pre}}$, can be described by a certain parametrized two-dimensional surface.

This is motivated by the intuition that the rates of scour depth and scour volume together convey some information about the bed elevation rate. For example, a hole that is in the process of being eroded at the pile base, as represented by a strong increase of the scour depth, but whose over-all volume only grows faintly, as represented by a weak increase of the scour volume, indicates that the bed elevation rate is strongly negative at the pile base but diminishes to zero in the remaining domain. The reason why the inference from dV/dt and dS/dt to $\partial h/\partial t$ is only *indicative* is the fact that a given scour depth rate and scour volume rate can both be fulfilled at the same time by *several* surfaces describing the bed elevation rate, but admittedly with some being more physically probable than others. In the predictor, the set of allowable surfaces are limited to a single general one that caters for both scouring and backfilling and allows the system of equations to be closed and solved.

The predictor bed elevation rate is described along a radial line by the use of polar coordinates. This offers a simple and clear geometrical interpretation of the surface and still allows angular variations when the radial

line is swept across all values of the angle. The spatial coordinates may be mapped between polar (r, θ) and Cartesian (x, y) coordinates by the use of conventional transformations. Finally, I will note that the predictor treats the bed elevation in the scour domain alone and leaves the ambient domain unaffected.

In the following sections, I present the radial description, the auxiliary equations and the relation between the scour volume rate and the predictor bed elevation rate. I have separated the *auxiliary conditions* from the other sections to clarify my presentation and assist possible future attempts to modify the existing auxiliary conditions or incorporate new ones. Finally, I present the bed update procedure, the choice of the time step and a flow chart over the predictor.

4.1. Radial description

The bed elevation rate in the scour domain is modeled by the following partial differential equation:

$$\left(\frac{\partial h}{\partial t}\right)_{\text{pre}} = b \cdot (1 - r_2^p)^{1/p}, \quad t > 0, \quad (r, \theta) \in \Omega \tag{4.1a}$$

or revealing the dependencies of the variables:

$$\left(\frac{\partial h(r,\theta,t)}{\partial t}\right)_{\text{pre}} = b\,(\theta, t) \cdot \left(1 - r_2\,(r, \theta, t)^{p(\theta,t)}\right)^{1/p(\theta,t)}, \quad t > 0, \quad (r, \theta) \in \Omega \tag{4.1b}$$

Above, b is the bed elevation rate at the pile base which is referred to as the *base elevation rate*, $p > 0$ is the curvature coefficient and r_2 is the normalized radius.

The normalized radius is given by:

$$r_2\,(r, \theta, t) = \frac{r - r_{\min}}{r_{\max}\,(\theta, t) - r_{\min}} \tag{4.2}$$

This ensures for any point inside the scour domain that $r_2 \in [0, 1]$ and consequently that $\partial h/\partial t$ is between b and 0, respectively. The surface formulation (4.1)-(4.2) implicitly fulfills the following two boundary conditions:

$$\begin{aligned} r = r_{\min} \quad &\Rightarrow \quad r_2 = 0 \quad \Rightarrow \quad (\partial h/\partial t)_{\text{pre}} = b \\ r = r_{\max} \quad &\Rightarrow \quad r_2 = 1 \quad \Rightarrow \quad (\partial h/\partial t)_{\text{pre}} = 0 \end{aligned}$$

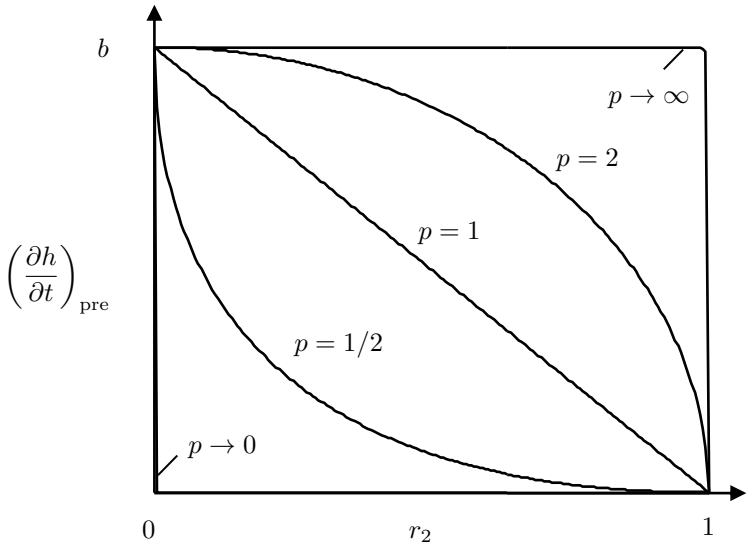

Figure 4.1: Predictor bed elevation rate along a radial line for varying curvature coefficients p

In words, the growth of the bed elevation at any point *at the pile base* is identical to the growth of b, while the bed elevation at any point *on the outer boundary* of the scour domain never changes. The variation between these two boundaries is prescribed by the curvature coefficient p. This is illustrated in Fig. 4.1 which shows the bed elevation rate along a radial line for different curvature coefficients. The physical interpretation of a decreasing curvature coefficient is erosion/deposition being concentrated closer to the pile, whereas an increasing curvature coefficient implies a more uniform distribution along the radial line.

On a final note, the formulation also imposes $\partial\left(\partial h/\partial t\right)/\partial r \leq 0$, i.e. a strictly decreasing or nil development in any radial direction away from the pile. This implies that the magnitude of erosion or deposition at any point cannot exceed that of a point closer to the pile. The auxiliary conditions are given in the following section.

4.2. Auxiliary conditions

In the previous section, I presented the four core parameters of the predictor, namely $r_{\min}$, $r_{\max}$, p and b. In this section, I will present some auxiliary conditions that are used to model some of these parameters. This

augmentation accommodates for the features of the scour hole or provide new parameters that can be more easily determined than the original ones. The augmentation yields the following ten parameters: $r_{\min}$, r_c, c_r, μ_s, c_g, p_c, c_p, b_c, c_b and f_b. Aside from $r_{\min}$ and μ_s, the remaining parameters are generally functions of time.

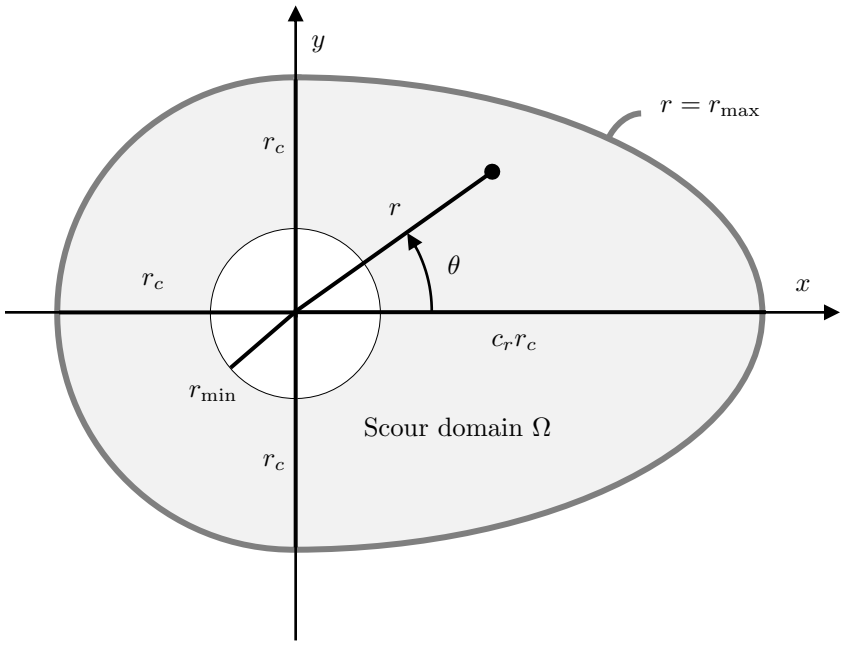

Figure 4.2: Definition of scour domain (shown in darker color)

4.2.1. Outer boundary of scour domain

The *outer* boundary $r = r_{\max}$ of the scour domain is assumed to follow a semi-circle in the upstream domain and a semi-ellipse in the downstream domain as inferred from feature 3. The scour domain is illustrated in Fig. 4.2. The radial extent of the outer boundary is given by:

$$r_{\max}(\theta, t) = \begin{cases} r_c(t) \cdot \left(\dfrac{\cos^2 \theta}{c_r(t)^2} + \sin^2 \theta \right)^{-1/2}, & -\pi/2 \leq \theta \leq \pi/2 \\ r_c(t), & \text{else} \end{cases} \tag{4.3}$$

Above, r_c is the outer radius in the upstream scour domain and is referred to as the *lateral* radius, $c_r r_c$ is the outer radius in the downstream di-

rection and c_r is an amplification factor. Generally, r_c and c_r are functions of time. The upper equation of (4.3) has been derived from the canonical definition of an ellipse in polar coordinates: $(r_{\max}\cos\theta)^2/(c_r r_c)^2+(r_{\max}\sin\theta)^2/{r_c}^2 = 1$. In the special case when $r_{\max}$, p and b do not vary with respect to the angle (i.e. $\partial r_{\max}/\partial\theta = \partial p/\partial\theta = \partial b/\partial\theta = 0$), the scour domain becomes circular and the bed elevation rate becomes axisymmetrical around the pile axis.

The formulation in (4.1)-(4.3) accommodates features 1-2 and allows the bed elevation rate to assume different shapes by tuning the curvature coefficient p. This is exemplified in Fig. 4.3 for different constant values of p. One obtains a tube in the lower limit $p \to 0$, a cone when $p = 1$, a hemisphere-hemiellipsoid when $p = 2$ and a filled cylinder in the upper limit $p \to \infty$. If p or b are allowed to vary with respect to the angle, as modeled later, the predictor bed elevation rate can assume an even more organic shape.

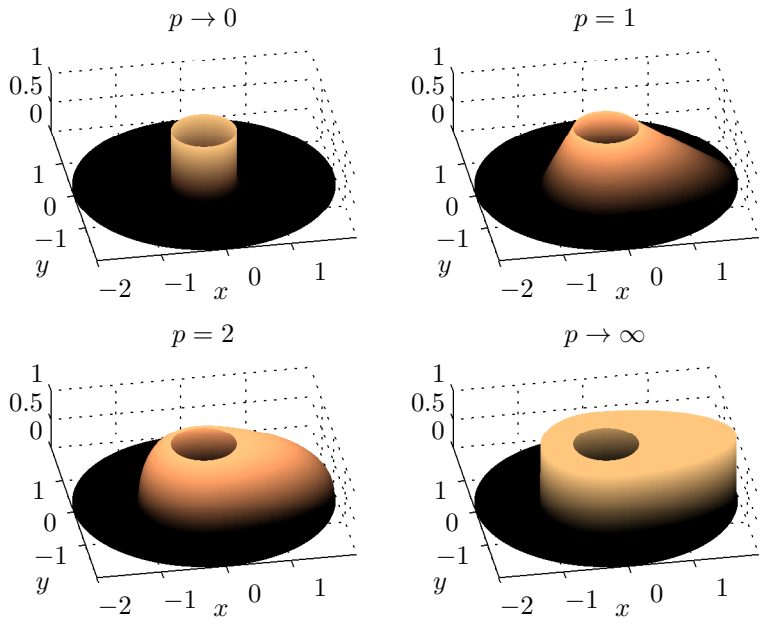

Figure 4.3: Examples of predictor bed elevation rate $(\partial h/\partial t)_{\text{pre}}$ for different values of the curvature coefficient p and $2r_{\min} = r_c = c_r/2 = b = 1$. The bed elevation rate outside the scour domain has been taken as zero (shown in black color)

4.2.2. Lateral radius and global sliding criterion

In this section, I propose an ordinary differential equation for describing the temporal development of the lateral radius r_c. The equation is based on the following assumptions:

- Sliding is assumed to play a leading role during scouring and a minor role during backfilling.
- Feature 1 suggests two principles. First, the rate of the lateral radius is approximately proportional to that of the scour depth during scouring, except when far from equilibrium. Secondly, the lateral radius appears to remain approximately constant with respect to time during backfilling. If the scour hole becomes sufficiently small at some moment in time, the lateral radius may be expected to decrease but I have found it difficult to confirm or quantify this and have therefore not offered it in this description.
- A limit state function (described below) can be inferred from the experimental bed surfaces of Hartvig et al. (2010), Dey and Barbhuiya (2005) and Link and Zanke (2004).

Alternative approaches that exploit existing information in the model could also have been employed and may be more accurate. Say, tracking the location and travel distance of sliding particles that enter or leave the scour domain in the corrector step, or devising an optimization rule that minimizes the difference between the current bed surface and an idealized scoured bed surface.

The experiments of Hartvig et al. (2010) approximately satisfy the following limit state function:

$$g_1 = \frac{c_g S}{r_c - r_{\min}} - \mu_s \tag{4.4}$$

with the following three interpretations:

$$\begin{array}{ll} g_1 > 0, & \text{unstable} \\ g_1 = 0, & \text{sliding} \\ g_1 < 0, & \text{stable} \end{array} \tag{4.5}$$

Above, g_1 is the limit state function for the entire scour hole, μ_s is the static coefficient of friction, $c_g S$ is the maximum depth at any point on the pile base and $c_g \geq 1$ is an amplification factor that takes into account that the maximum depth may deviate from the scour depth since the latter is

a mean quantity in this framework. The sliding criterion specified by Eqs. (4.4)-(4.5) is referred to as the *global* sliding criterion, in order to distinguish it from the *local* sliding criterion introduced in Sec. 5.1.

If sliding occurs, the middle equation of (4.5) is fulfilled and we can rearrange (4.4) to obtain:

$$r_c = \frac{c_g S}{\mu_s} + r_{\min} \tag{4.6}$$

Eq. (4.6) can be differentiated with respect to time while regarding μ_s and $r_{\min}$ as constants. This provides the following ordinary differential equation for steering the rate of the lateral radius:

$$\frac{dr_c}{dt} = \begin{cases} \frac{1}{\mu_s} \cdot \frac{d\left(c_g S\right)}{dt}, & g_1 \geq 0 \\ 0, & \text{else} \end{cases}, \quad t > 0 \tag{4.7}$$

The amplification factor c_g can be obtained by probing the bed elevation h at the pile base at the current time step:

$$c_g(t) = \max\left\{1, \frac{\max h(r = r_{\min}, \theta, t)}{-S(t)}\right\} \tag{4.8}$$

In practice, dc_g/dt is assumed to be negligible and therefore the upper equation of (4.7) reduces to $dr_c/dt \approx dS/dt\ c_g/\mu_s$ for $g_1 \geq 0$. To facilitate another usage of this latter equation, the scour depth rate is made absolute as shown in Fig. 4.7.

4.2.3. Curvature coefficient

Based on features 1-2, the curvature coefficient is allowed to vary with the angle. Keeping feature 5 in mind too, the curvature coefficient is modeled piece-wisely with a 3rd degree spline and a constant as:

$$p(\theta, t) = \begin{cases} p_c(t) \cdot \left(c_p(t) + (1 - c_p(t)) \left(\frac{12}{\pi^2} |\theta|^2 - \frac{16}{\pi^3} |\theta|^3\right)\right), & -\pi/2 \leq \theta \leq \pi/2 \\ p_c(t), & \text{else} \end{cases} \tag{4.9}$$

Here, p_c is the curvature coefficient of the upstream scour domain, $c_p p_c$ is the curvature coefficient in the downstream direction and c_p is an amplification factor. The bars denote absolute value and p_c and c_p are generally functions of time. The curvature coefficient with respect to the angle is shown in Fig. 4.4 and the influence of the c_p factor for a fixed p_c on the

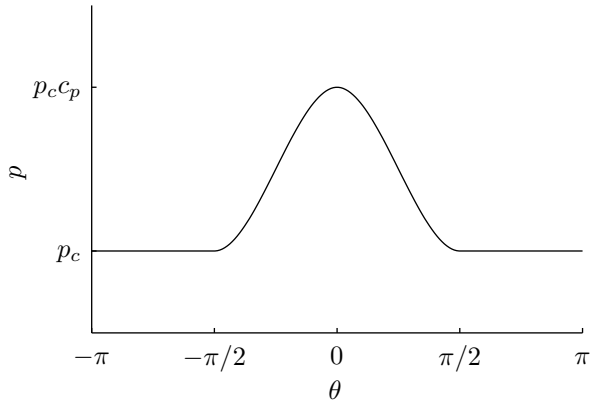

Figure 4.4: Curvature coefficient as function of angle

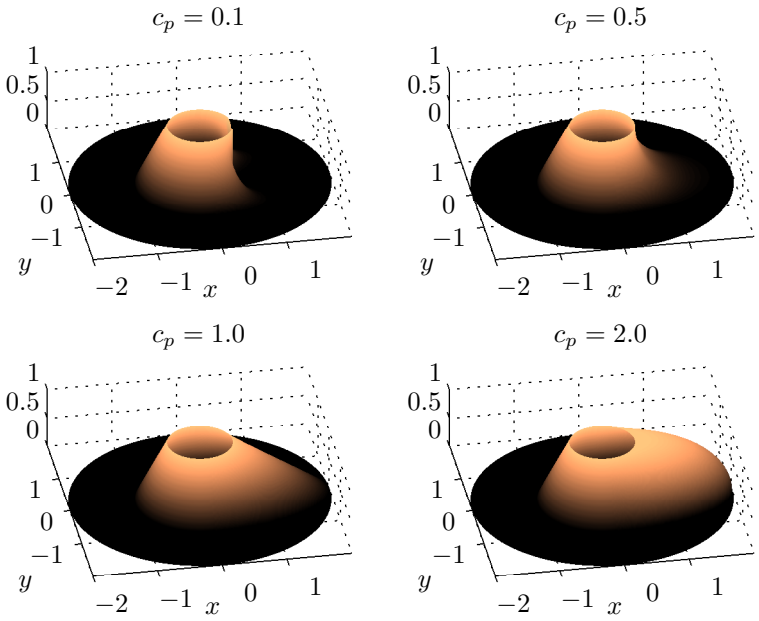

Figure 4.5: Examples of predictor bed elevation rate $(\partial h/\partial t)_{\text{pre}}$ for different values of the curvature amplification factor c_p and $2r_{\min} = r_c = c_r/2 = p_c = b = 1$

predictor bed elevation rate is illustrated in Fig. 4.5. The spline on the upper right-hand-side of (4.9) is used for the downstream scour domain and implicitly satisfies the following four boundary conditions:

$$\begin{aligned} |\theta| = 0 \quad &\Rightarrow \quad p = p_c c_p \\ |\theta| = \pi/2 \quad &\Rightarrow \quad p = p_c \\ |\theta| = 0 \quad &\Rightarrow \quad \partial p/\partial\theta = 0 \\ |\theta| = \pi/2 \quad &\Rightarrow \quad \partial p/\partial\theta = 0 \end{aligned}$$

The two last boundary conditions involving the differentials ensure a smooth transition at the angles where the matching occurs. A unity amplification factor $c_p = 1$ implies that the curvature coefficient is also constant with respect to the angle in the downstream scour domain, i.e. $p = p_c$ and $\partial p/\partial\theta = 0$ everywhere in the scour domain.

4.2.4. Base elevation rate

To capture feature 4 and 5, the base elevation rate is assumed to vary in a similar fashion as the curvature coefficient as derived above, yielding similarly:

$$b(\theta, t) = \begin{cases} b_c(t) \cdot \left(c_b(t) + (1 - c_b(t)) \left(\frac{12}{\pi^2} |\theta|^2 - \frac{16}{\pi^3} |\theta|^3 \right) \right), & -\pi/2 \leq \theta \leq \pi/2 \\ b_c(t), & \text{else} \end{cases} \tag{4.10}$$

where b_c is the base elevation rate along the pile base in the upstream scour domain, $c_b b_c$ is the base elevation rate in the downstream direction and c_b is an amplification factor.

4.2.5. The scour depth rate and the integrated base elevation rate

The previous modification allowed the base elevation rate b to deviate from the scour depth rate $(dS/dt)_{\text{pre}}$. However, as suggested by (2.1), the magnitude of the base elevation rate averaged along the pile base must equate that of the scour depth rate:

$$\left(\frac{dS}{dt} \right)_{\text{pre}} = -\frac{1}{2\pi} \int_{-\pi}^{\pi} b \, d\theta \tag{4.11}$$

Evaluating the integral in (4.11) with the line-spline formulation for the base elevation rate (4.10) yields:

$$\left(\frac{dS}{dt}\right)_{\text{pre}} = -b_c \cdot \left(\frac{c_b}{4} + \frac{3}{4}\right) \tag{4.12}$$

To determine the upstream base elevation rate b_c, I assume that the magnitude of b_c is proportional to the predictor scour depth rate:

$$b_c = -f_b \cdot \left(\frac{dS}{dt}\right)_{\text{pre}} \tag{4.13}$$

where $f_b > 0$ is a parameter that may change with time. Combining (4.12) and (4.13) gives the following relation for the c_b parameter:

$$c_b = \frac{4}{f_b} - 3 \tag{4.14}$$

If $f_b > 1$, the magnitude of the base elevation rate is greater upstream than downstream, simulating that erosion/deposition is stronger at upstream points than downstream points. If $f_b = 1$, this implies that $c_b = 1$ and $b = b_c = -\left(dS/dt\right)_{\text{pre}}$ and thus, the bed elevation rate at any point at the pile base is equal in magnitude to the scour depth rate. The influence of f_b is illustrated in Fig. 4.6.

4.3. The scour volume rate and the integrated bed elevation rate

As suggested by (2.2), the local rate of the bed elevation can be integrated with respect to the area of the scour domain to provide the scour volume rate dV/dt. Exploiting the symmetry about the streamwise axis, this can be expressed as:

$$\left(\frac{dV}{dt}\right)_{\text{pre}} = -2\int_{\theta=0}^{\theta=\pi}\int_{r=r_{\min}}^{r=r_{\max}(\theta)} \left(\frac{\partial h}{\partial t}\right)_{\text{pre}} r\, dr d\theta \tag{4.15}$$

When the left-hand-side is given, the value of p_c that satisfies the equation is found by the bisection method. The double integral in (4.15) is evaluated numerically by an adaptive quadrature scheme. I have determined the analytical solutions to (4.15) for some special cases by the use of (4.1)-(4.3), (4.11) and reproduced them below for validation purposes:

$$\left(\frac{\dfrac{dV}{dt}}{\dfrac{dS}{dt}}\right)_{\text{pre}} = \begin{cases} 0, & p \to 0 \\ \frac{\pi}{3}\left(r_c^2 + r_c r_{\min} - 2r_{\min}^2\right), & p = 1, \quad c_b = c_r = 1 \\ \frac{\pi}{6}\left(4r_c^2 + (3\pi - 8)\, r_c r_{\min} - (3\pi - 4)\, r_{\min}^2\right), & p = 2, \quad c_b = c_r = 1 \\ \frac{\pi}{2}\left(r_c^2 + c_r r_c^2 - 2r_{\min}^2\right), & p \to \infty, \quad c_b = 1 \end{cases}$$

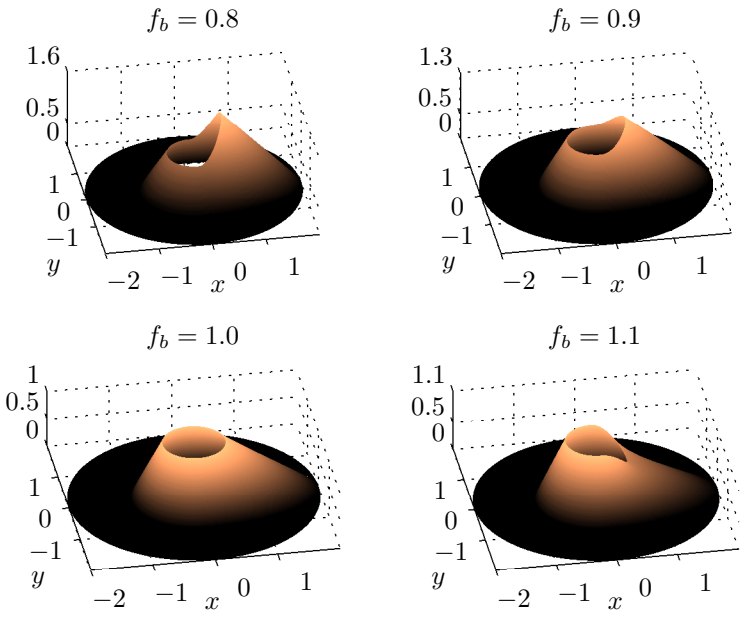

Figure 4.6: Examples of predictor bed elevation rate $(\partial h/\partial t)_{\text{pre}}$ for different values of f_b and $2r_{\min} = r_c = c_r/2 = p = -(dS/dt)_{\text{pre}} = 1$

4.4. Bed update and time step

The bed elevation can be determined by integrating (3.1a) numerically with respect to time. For the sake of simplicity, the forward Euler scheme has been adopted for this and most other numerical temporal integrations and can be written as:

$$h(r,\theta,t+\Delta t) \approx h(r,\theta,t) + \frac{\partial h(r,\theta,t)}{\partial t}\Delta t \tag{4.16}$$

where $\partial h(r,\theta,t)/\partial t$ in the second term is given by (3.1a) and $\Delta t > 0$ is the time step.

The time step is adjusted at each time step based on several considerations. On one hand, it should be as large as possible for the sake of computational efficiency. On the other hand, it must be small enough to avoid dramatic changes of the bed elevation to ensure the accuracy of the temporal integration in (4.16). It must also be small enough to avoid dramatic changes of the bed elevation *gradient* to ensure the stability of the corrector. If the gradient of the bed elevation changes too much in the predictor step, beyond the working range of the corrector one might say, the corrector step will introduce an erroneous checkerboard pattern into the bed elevation. With these considerations in mind, the time step is chosen as:

$$\Delta t = \min \begin{cases} \dfrac{(\Delta h)_{\text{pre,max}}}{\max|b_c, b_c c_b|}, & c_b b_c \neq 0 \\ \dfrac{c_{\mu 1}\,\mu_s}{\max\left|\dfrac{\partial\,(\partial h/\partial t)_{\text{pre}}}{\partial x_\alpha}\right|} \end{cases} \tag{4.17}$$

where $(\Delta h)_{\text{pre,max}} > 0$ is the maximum allowable growth of the bed elevation in a predictor step. The bottom criterion and its specific parameters $c_{\mu 1}$ and the gradient of the predictor bed elevation rate $\partial\,(\partial h/\partial t)_{\text{pre}}/\partial x_\alpha$ pertain to the predictor but are conceptually identical to those introduced in the corrector and therefore a more detailed explanation awaits there, especially in Sec. 5.4 on the inner time step of the corrector. The magnitude of the gradient is computed numerically like those in the corrector, see Sec. 5.1 and Sec. 5.5. In practice, a third criterion enters (4.17) that adjusts the time step to allow the next iteration to arrive exactly at a prescribed time, so the bed surface can be extracted at given measuring time stations regardless of the time step history.

The corrector rate of the scour depth is approximated as the following finite difference:

$$\left(\frac{dS}{dt}\right)_{\text{cor}} \approx \frac{S_{\text{new}} - S_{\text{old}}}{\Delta t}$$

where the scour depths are computed according to (2.1) and the subscripts 'new' and 'old' denote a computation *after* and *before* the corrector step, respectively, as illustrated in Fig. 5.2. A similar approach can be used for the scour volume, but in practice, this has not been carried out since the corrector rate of the scour volume is expected to be negligible, i.e. $(dV/dt)_{\text{cor}} \approx 0$.

4.5. Flow chart

In order to close the system of equations, model variables are to be prescribed at the initial time instance $t = t_0$ as *initial* conditions, prescribed at every time step as *boundary* conditions or *solved* for by the equations of the predictor. The classification of the variables depend on the problem and one case is visualized in the flow chart in Fig. 4.7. In this case, the initial conditions encompass the lateral radius $r_{c0} = r_c(t = t_0)$ and the bed elevation $h_0 = h(r, \theta, t = t_0)$. The boundary conditions encompass dV/dt, dS/dt, S, $r_{\min}$, c_r, μ_s, c_g, c_p and f_b as well as $c_{\mu 1}$ and $(\Delta h)_{\text{pre,max}}$ for the temporal resolution. The variables to be solved are r_c, p_c, b_c and c_b by the use of Eqs. (4.7), (4.15), (4.13) and (4.14), respectively.

As seen in Fig. 4.7, the procedure increases the lateral radius r_c until the hole is stable against global sliding and the predictor scour volume rate can be fulfilled by a certain choice of p_c. Thus, it corrects a poor user-definition of the initial lateral radius r_{c0} and also detects at later instances during the simulation if the scour volume rate cannot be fulfilled by the present r_c, e.g. when the magnitude of the rate of the scour depth is small compared to that of the scour volume.

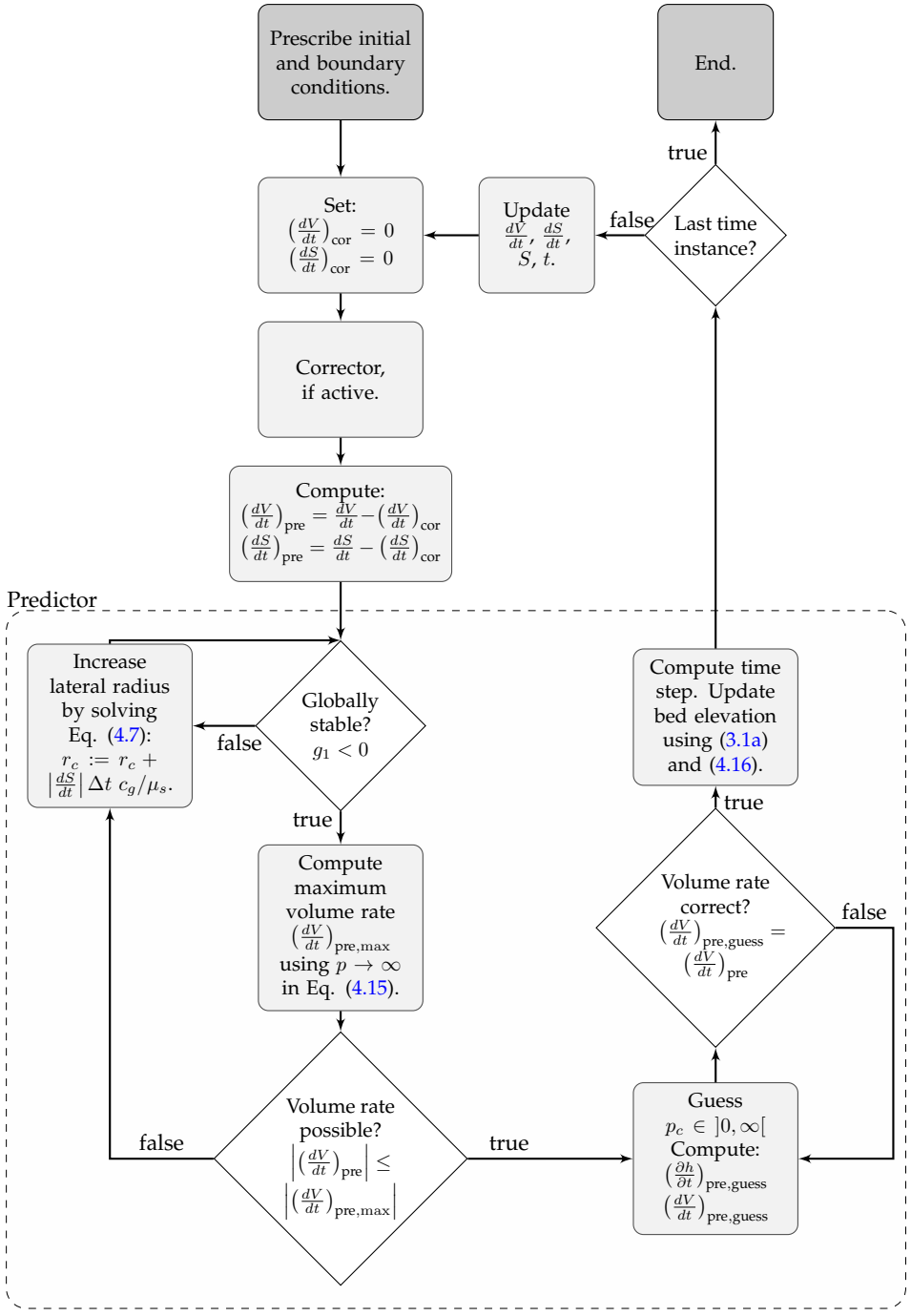

Figure 4.7: Flow chart of computations in predictor. It is implicit in the notation here that all variables are evaluated at the current time step

5. Corrector

The corrector adjusts the bed surface for effects of sliding. It is based on the following general assumptions:

- The bed material is incompressible and its mass or volume is conserved. These assumptions are inherent in the Exner equation and it therefore serves as a convenient framework that facilitates sliding while conserving the bed load volume.
- Each bed particle is assumed to be subjected only to quasi-static forces and only the *driving* force of gravity reduced for effects of buoyancy and the *resisting* forces of friction and fluid drag in *still* water. Therefore, inertia of the moving particles, collisions between particles, mutual influence of neighboring particles on the fluid forces, influence of the fluid velocity on the drag force and all unsteady effects are some of the phenomena not considered.
- Sliding occurs instantaneously. This approximation implies that the time step in the Exner equation becomes an internal or pseudo-nature time step that can be chosen freely. I exploit this freedom to eliminate some of the physical parameters of the sliding procedure that are constant with respect to space as detailed later. In practice, this allows the corrector to depend only on two physical parameters, namely the static and dynamic coefficients of friction, μ_s and μ_d, respectively.

The corrector differs from the predictor in two respects. Firstly, it is entirely numerical and is approximated on a spatial grid which governs its performance. Secondly, the corrector is allowed to operate on the entire bed domain, not just the scour domain, although the corrector can only influence the scour domain and nodes that flank its borders after the initial time step since the predictor only influences the scour domain.

The bed domain is defined between the inner boundary of the scour domain, $r = r_{\min}$ comprised of the *inner* nodes, and a user-defined outer boundary comprised of *outer nodes*, ideally selected such that the bed domain completely covers the scour domain. The intermediate domain is comprised of *interior* nodes as illustrated in Fig. 5.1.

In the following sub sections, the four elements of the corrector are described: The local sliding criterion, the bed update, the bed velocity and the inner time step. Afterwards, the spatial grid is presented together with a brief description of how the gradient and divergence operators have been

approximated in polar coordinates. The section is concluded with a flow chart over the corrector.

5.1. Local sliding criterion

Local sliding is assumed to be described by the following limit state function:

$$g_2 = \left| \frac{\partial h}{\partial x_\alpha} \right| - \mu_s, \quad r > r_{\min} \tag{5.1}$$

with the criteria:

$$\begin{array}{ll} g_2 > 0, & \text{unstable} \\ g_2 = 0, & \text{sliding} \\ g_2 < 0, & \text{stable} \end{array} \tag{5.2}$$

Eqs. (5.1)-(5.2) are referred to as the *local* sliding criterion. g_2 is the local limit state function in the two-dimensional space for every node in the bed domain except the inner nodes at the pile perimeter. The reason for excluding the inner nodes is given in the next section. This is different from g_1 which pertains to parameters of the scour domain only and considers the scour hole as a whole, not node-wise. $\partial h/\partial x_\alpha$ is the two-dimensional gradient vector of the bed elevation and its magnitude – the first term on the right-hand-side of (5.1) – is precisely the *bed slope*, i.e. the unsigned slope of the steepest tangential plane of the bed relative to a horizontal plane. Introducing the *angle* of the bed slope – referred to as the *slope angle* ϕ:

$$\phi = \tan^{-1} \left| \frac{\partial h}{\partial x_\alpha} \right| \tag{5.3}$$

it becomes clear that the local limit state function (5.1) is equivalent to a more conventional criterion that assumes sliding to occur when the slope angle exceeds the repose angle $\phi_r = \tan^{-1} \mu_s$. When the middle or upper equations of (5.2) are satisfied at any of the considered nodes, one or more *sliding* iterations are carried out until the bed is stable again when the lower equation of (5.2) is satisfied at all the considered nodes. The series of iterations are referred to as the *sliding procedure*. The stopping criterion that I adopt here is slightly simpler than in Roulund et al. (2005) who assumed that the sliding procedure terminates when the slope angle has decreased to less than a few degrees smaller than the repose angle and thus simulates "oversteepening". This has not been done here due to brevity.

In order to derive a purely polar formulation, the magnitude of the gradient vector is expanded into its *polar* rather than Cartesian scalar projections, using the following identity:

$$\left|\frac{\partial h}{\partial x_\alpha}\right| = \left|\left(\frac{\partial h}{\partial r}, \frac{1}{r}\frac{\partial h}{\partial \theta}\right)\right| = \sqrt{\left(\frac{\partial h}{\partial r}\right)^2 + \frac{1}{r^2}\left(\frac{\partial h}{\partial \theta}\right)^2} \tag{5.4}$$

The magnitude of the gradient vector is computed as the square root term in (5.4). The finite approximations of the polar components $\partial h/\partial r$ and $\partial h/\partial \theta$ are computed as detailed in Sec. 5.5.

5.2. Bed update

Writing the Exner equation (1.1) without sink terms leads to the following equation that conserves the bed load, enforcing erosion at departure nodes and deposition at arrival nodes as the grains slide from their original position:

$$\frac{\widehat{\partial h}}{\partial t} = \frac{1}{\kappa - 1}\frac{\partial Q_\alpha}{\partial x_\alpha}, \quad \widehat{t} > 0 \tag{5.5}$$

where $\widehat{\partial h/\partial t}$ is the bed elevation rate during a sliding iteration, Q_α is the bed flux vector due to sliding and $\widehat{t}$ is the *inner* time during sliding iterations, being nil at the initiation of a sliding procedure and $\widehat{t}_{\max}$ at the termination of the procedure. Integrating the Exner equation (5.5) provides the equation for the corrector bed elevation rate:

$$\left(\frac{\partial h}{\partial t}\right)_{\text{cor}} = \lim_{\Delta t \to 0} \frac{1}{\Delta t} \int_{\widehat{t}=0}^{\widehat{t}_{\max}} \frac{\widehat{\partial h}}{\partial t}\, \widehat{dt} \tag{5.6}$$

The integral in (5.6) represents the total change of bed elevation due to sliding when all sliding iterations have been performed in a corrector step. In practice, the integral is evaluated numerically by iterating through each slide step by the forward Euler scheme:

$$\widehat{\Delta h} \approx \frac{\widehat{\partial h}}{\partial t}\, \widehat{\Delta t} \tag{5.7}$$

where $\widehat{\Delta h}$ is the bed elevation growth during a single sliding iteration and $\widehat{\Delta t}$ is the inner time step. If the bed layer is composed of a single layer of spherical particles, the bed flux vector due to sliding can be assumed to follow:

$$Q_\alpha = \frac{\frac{\pi}{6}d^3}{d^2} \cdot U_\alpha$$

where the denominator expresses the area of the control area and U_α is the bed velocity, yielding:

$$\widehat{\Delta h} \approx \frac{\pi d\, \widehat{\Delta t}}{6\,(\kappa - 1)} \cdot \frac{\partial U_\alpha}{\partial x_\alpha}$$

It is now apparent that the fraction $\pi d\widehat{\Delta t}/\left(6\,(\kappa-1)\right)$ controls the growth of the bed elevation during each sliding iteration, amplifying the spatial variation of the bed velocity divergence. When d and κ are constant with respect to space, they can be eliminated from the equations. This is because we are free to absorb their constant contribution into the inner time step due to the pseudo-time nature of the sliding procedure. In this case, (5.5) is equivalently replaced by:

$$\frac{\widehat{\partial h}}{\partial t} = -1\mathrm{m} \cdot \frac{\partial U_\alpha}{\partial x_\alpha}, \quad \widehat{t} > 0 \tag{5.8}$$

and (5.7) is computed based on this. The bed velocity and the inner time step is described in the following sections and the finite approximation of the velocity divergence $\partial U_\alpha/\partial x_\alpha$ is detailed in Sec. 5.5.

5.3. Bed velocity

Consider a spherical particle as it slides down the bed with presumingly constant speed along a linear path. Following Newton's 1st law, the external static forces in the direction of particle motion must be in equilibrium:

$$F_{g\|U} - F_d - F_f = 0 \tag{5.9}$$

where $F_{g\|U}$ is the gravity force in the direction of motion reduced for effects of buoyancy, F_d is the drag force and F_f is the friction force, the two latter forces being in opposite direction of $F_{g\|U}$. The reduced gravity, drag and friction forces are given by:

$$\begin{aligned} F_g &= \frac{\pi}{6}d^3\rho g \cdot (s-1) \\ F_d &= \frac{\pi}{4}d^2\frac{1}{2}\rho c_d U^2 \\ F_f &= \mu_d F_{g\perp U} \end{aligned} \tag{5.10}$$

where F_g is the reduced gravity force in downwards direction, g is the acceleration due to gravity, d is the diameter of the spherical grain, ρ is the density of water, $s = \rho_s/\rho$ is the relative grain-water density and ρ_s is the density of the solid grain. Also, c_d is the drag coefficient, U is the speed of the grain, μ_d is the dynamic coefficient of friction, fulfilling $\mu_d < \mu_s$. $F_{g\perp U}$ is the reduced gravity force normal to the bed and can be determined by decomposing F_g into the direction of motion and normal to the motion:

$$\begin{pmatrix} F_{g\parallel U} \\ F_{g\perp U} \end{pmatrix} = F_g \cdot \begin{pmatrix} \sin\phi \\ \cos\phi \end{pmatrix} \tag{5.11}$$

In order to satisfy conservation of bed load and prohibit particles from sliding *through* the pile interface, particles at the pile perimeter that potentially could slide must have no velocity in the radial direction, i.e. $U_r = 0$. For the sake of simplicity, particles at the pile perimeter are assumed to have no velocity at all and thus are unable to slide. I emphasize that this does not hinder the bed elevation at the pile perimeter from changing, since $U = 0$ does not necessarily imply that the bed velocity is divergence-less at the perimeter, $\partial U_\alpha/\partial x_\alpha = 0$.

Using Eqs. (5.9)-(5.11) for sliding particles and $U = 0$ for particles that are stable or located at the pile perimeter, the particle speed of each node can be determined as:

$$U = \begin{cases} \sqrt{\dfrac{(\sin\phi - \mu_d\cos\phi)\,8F_g}{\pi d^2 \rho c_d}}, & g_2 \geq 0 \text{ and } r > r_{\min} \\ 0, & \text{else} \end{cases} \tag{5.12}$$

The pseudo-time nature of the sliding procedure eliminates any of the parameters on the right-hand-side of (5.12) that are constant with respect to space. Thus, if F_g, d, ρ, c_d can be assumed to be constant with respect to space, Eq. (5.12) may equivalently be replaced by the following formulation:

$$U = \begin{cases} 1\frac{\mathrm{m}}{\mathrm{s}} \cdot \sqrt{\sin\phi - \mu_d\cos\phi}, & g_2 \geq 0 \text{ and } r > r_{\min} \\ 0, & \text{else} \end{cases} \tag{5.13}$$

As an approximation, one could in fact entirely drop the dependence of the bed velocity on the slope angle, i.e.:

$$U = \begin{cases} 1\frac{\mathrm{m}}{\mathrm{s}}, & g_2 \geq 0 \text{ and } r > r_{\min} \\ 0, & \text{else} \end{cases}$$

but this is not recommended since it is less physical and appears to increase the number of sliding iterations.

Sliding particles are assumed to travel *down* the steepest bed slope as dictated by the static force equilibrium that was previously presented. Accounting for the attribute that $\partial h/\partial x_\alpha$ points *up* the bed slope, the bed velocity vector U_α must point in the direction of $-\partial h/\partial x_\alpha$. Decomposing the bed velocity vector into its polar components U_r and U_θ rather than Cartesian components U_α, I obtain:

$$\begin{pmatrix} U_r \\ U_\theta \end{pmatrix} = -U \cdot \begin{pmatrix} \cos\theta_2 \\ \sin\theta_2 \end{pmatrix} \tag{5.14}$$

where U_r and U_θ are the scalar projections of the bed velocity vector U_α and unit vectors pointing in the positive radial direction r and rotated 90 degrees counter-clock-wise relative to the positive radial direction, respectively. θ_2 is the signed counter-clock-wise angle of the gradient vector relative to the positive radial direction, given by:

$$\theta_2 = \text{atan2}\left(y_2 = \frac{1}{r}\frac{\partial h}{\partial \theta}, x_2 = \frac{\partial h}{\partial r}\right) \tag{5.15}$$

where $\text{atan2}(y_2, x_2)$ is the two-argument arctangent function in the range $[-\pi, \pi]$, in contrast to the conventional one-argument arctangent function $\tan^{-1}(y_2/x_2)$ in the range $[-\pi/2, \pi/2]$.

5.4. Inner time step

The inner time step is varying during each sliding iteration and is chosen to satisfy an *inner time step criterion* given for every node as:

$$\left|\frac{\partial\left(\widehat{\Delta h}\right)}{\partial x_\alpha}\right| - c_{\mu 2}\,\mu_s \leq 0 \tag{5.16}$$

Above, $\partial(\widehat{\Delta h})/\partial x_\alpha$ is the gradient of the bed elevation growth and its magnitude can be interpreted as the unsigned slope of the bed elevation growth $\widehat{\Delta h}$ and is referred to as the *relative slope*. $c_{\mu 2}\,\mu_s$ is the maximum allowable relative slope and $c_{\mu 2} > 0$ is a computational slope parameter. As an example for $\mu_s = 0.62$, the slope parameter $c_{\mu 2} = 0.10$ corresponds to limiting the angle of the relative slope to be at most 3.5 degrees at each node during a sliding iteration. Rearranging (5.16) and using (5.7), the inner time step is computed as the largest possible value that satisfies the inner time step criterion and is given as:

$$\widehat{\Delta t} = \frac{c_{\mu 2}\ \mu_s}{\max \left| \dfrac{\partial \left(\widehat{\partial h / \partial t} \right)}{\partial x_\alpha} \right|} \tag{5.17}$$

The criterion in (5.17) ensures that the bed elevation growth during a sliding iteration is large enough to be resolved in the subsequent computation of the bed gradient and yet small enough to avoid dramatic changes of the slope angle during a sliding iteration which could misguide the solution. In other words, the criterion is sensitive to the *magnitude of the gradient* of the bed elevation growth rather than the bed elevation growth itself. Thus, it restricts dramatic changes of the bed elevation *relatively between* neighboring nodes (which affect the slope angle) but allows dramatic changes occurring simultaneously in neighboring nodes (which increases the bed elevation but does not affect the slope angle).

In some respects, the criterion resembles a conventional Courant-Friedrichs-Lewy (CFL) criterion for numerical spatio-temporal problems. However, a pure CFL criterion does not apply here due to the pseudo-time nature of the sliding procedure.

5.5. Spatial grid and operator approximations

The gradient of the bed elevation and the divergence of the bed velocity is approximated on a spatial grid that is shaped like a spider-web as suggested in Fig. 5.1. This distribution of nodes caters for a polar formulation and refines the resolution near the pile and in the scour domain which is the domain of interest here. The angle is distributed evenly as:

$$\theta_{j_\theta} = \Delta\theta \cdot (j_\theta - 1) - \pi, \quad j_\theta = 1, 2, \ldots, n_\theta$$

where $\Delta\theta = 2\pi / n_\theta$ is the angle increment and j_θ, n_θ are the actual and maximum number of nodes along the angular coordinate, respectively. To obtain the most accurate computation of the divergence, the cells must be nearly square and thus, the radius should grow as $dr = r\ d\theta$ since the arc length is known to grow as $dl = r\ d\theta$. This is fulfilled if the radius is distributed as the following geometric sequence with the radius at the inner boundary of the bed domain specified as $r_{\min}$:

$$r_{j_r} = r_{\min} \cdot (1 + \Delta\theta)^{j_r - 1}, \quad j_r = 1, 2, \ldots, n_r$$

where j_r and n_r are the actual and maximum number of nodes in the radial direction, respectively, and the latter controls the radial extent of the outer boundary of the bed domain.

5.5.1. Gradient

The approximation of the gradient vector is computed with a mix of two-nodal finite differences. The gradient of a scalar function h with respect to the *angle* is approximated by central differences which follows this pattern using the definitions in Fig. 5.1:

$$\begin{aligned}
\left(\frac{\partial h}{\partial \theta}\right)_A &\approx \frac{h_G - h_F}{2\Delta\theta} && \text{Inner nodes} \\
\left(\frac{\partial h}{\partial \theta}\right)_C &\approx \frac{h_I - h_H}{2\Delta\theta} && \text{Interior nodes} \\
\left(\frac{\partial h}{\partial \theta}\right)_E &\approx \frac{h_K - h_J}{2\Delta\theta} && \text{Outer nodes}
\end{aligned}$$

The gradient in the *radial* direction is approximated by *forward* differences for inner nodes, *central* differences for interior nodes and *backward* differences for outer nodes, i.e.:

$$\begin{aligned}
\left(\frac{\partial h}{\partial r}\right)_A &\approx \frac{h_B - h_A}{r_B - r_A} && \text{Inner nodes} \\
\left(\frac{\partial h}{\partial r}\right)_C &\approx \frac{h_D - h_B}{r_D - r_B} && \text{Interior nodes} \\
\left(\frac{\partial h}{\partial r}\right)_E &\approx \frac{h_E - h_D}{r_E - r_D} && \text{Outer nodes}
\end{aligned}$$

5.5.2. Divergence

In polar coordinates, the divergence of a two-dimensional vector field U_α can be expressed as:

$$\frac{\partial U_\alpha}{\partial x_\alpha} = \frac{\partial U_x}{\partial x} + \frac{\partial U_y}{\partial y} = \frac{\partial U_r}{\partial r} + \frac{1}{r} \cdot \left(\frac{\partial U_\theta}{\partial \theta} + U_r\right) \tag{5.18}$$

Instead of computing the divergence by the right-most equation of (5.18), a different formulation is used. This is based on the equivalent definition of the divergence which considers the flux of the vector quantity through the boundary of an infinitesimal two-dimensional control area:

$$\frac{\partial U_\alpha}{\partial x_\alpha} = \lim_{\lambda \to 0} \left(\frac{1}{\lambda} \int_Z U_\alpha n_\alpha \, d\zeta\right) \tag{5.19}$$

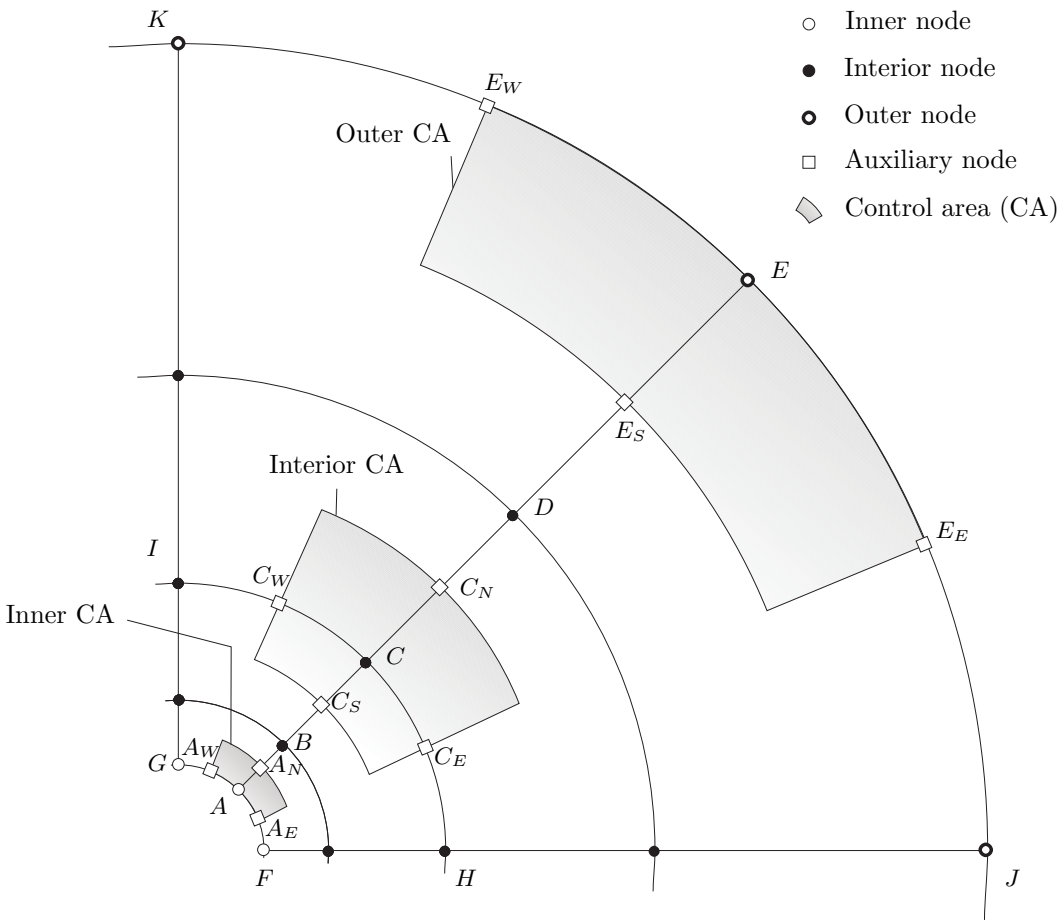

Figure 5.1: Example of spatial grid with $n_\theta = 8$ and $n_r = 5$ (entire grid not shown). The auxiliary nodes and control areas are used for computing the divergence. The indices N, W, S and E, denote the auxiliary nodes at the northern, western, southern and eastern side of the control area, respectively

Above, Z is a curve that completely encloses the control body, $d\zeta$ is an infinitesimal portion of this curve, n_α is the unit vector normal to the curve and directed outwards and λ is the area within the closed curve. Taking the interior control area in Fig. 5.1 as an example, the finite approximations of (5.19) for the interior nodes follow this pattern:

$$\left(\frac{\partial U_\alpha}{\partial x_\alpha}\right)_C \approx \frac{\Delta\theta \cdot (U_{rC_N} r_{C_N} - U_{rC_S} r_{C_S}) + \Delta r_C \cdot (U_{\theta C_W} - U_{\theta C_E})}{\Delta r_C \, \Delta\theta \, r_C} \tag{5.20}$$

where $\Delta r_C = (r_D - r_B)/2$ is the radius increment. The radii and normal scalar projections of the vector quantity at the borders of the control area – at the northern, western, southern and eastern auxiliary nodes – are estimated by linear interpolation from the neighboring nodes. Then, (5.20) reduces to:

$$\left(\frac{\partial U_\alpha}{\partial x_\alpha}\right)_C \approx \frac{U_{r\langle C,D\rangle} r_{\langle C,D\rangle} - U_{r\langle C,B\rangle} r_{\langle C,B\rangle}}{\Delta r_C \, r_C} + \frac{U_{\theta\langle C,I\rangle} - U_{\theta\langle C,H\rangle}}{\Delta\theta \, r_C} \tag{5.21}$$

where $f_{\langle A,B\rangle} \equiv (f_A + f_B)/2$ is a compressed notation to denote the mean value of the scalar function f at nodes A and B and f is U_r, U_θ or r.

The inner and outer nodes follow the pattern in (5.21) with a few differences. The radius increment is taken as $\Delta r_A = (r_B - r_A)/2$ for inner nodes and $\Delta r_E = (r_E - r_D)/2$ for outer nodes. Furthermore, the contribution of the southern border is omitted for inner nodes since $U_{rA} = 0$. For outer nodes, there may be a contribution at the northern border and the northern auxiliary node is taken as the node itself, i.e. $f_{E_N} = f_E$, as illustrated by the outer control area in Fig. 5.1.

5.6. Flow chart

The flow chart for the corrector is shown in Fig. 5.2. In conjunction with Fig. 4.7, the two flow charts illustrate the complete numerical scheme of the present model.

6. Comparison and discussion

In the previous sections, I presented the different aspects of the model. In this section, I evaluate its hindcasting performance. First, I present an overview of the simulations and chosen performance indicators. Then, I discuss the performance.

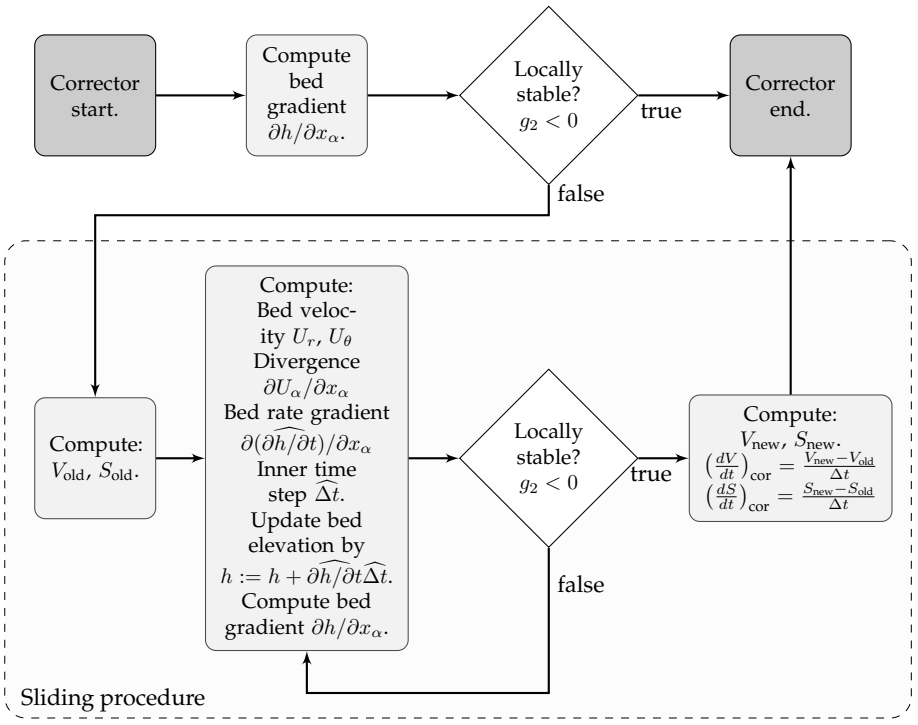

Figure 5.2: Flow chart of computations in corrector. It is implicit in the notation here that all variables are evaluated at the current time step

I have run nine simulations to assess the model performance in various scenarios. During each simulation, the simulated bed surface and relevant model parameters are stored at the four measuring time stations $t \in t_m$ with $m = 0, 1, 2, 3$ which are moments in time when experimental data on the bed surface from Hartvig et al. (2010) is available. Once a simulation has finished, the measured and simulated bed surface at each measuring time station are compared *qualitatively* based on plots of the bed elevation along cross-sections and *quantitatively* based on error measures as detailed in the following section.

The simulations and model parameters are given in Table 6.1. The B or S in the simulation name denotes backfilling or scouring, respectively. The pairs of simulation with the same first digit are meant to contrast each other and expose a certain aspect of the model as discussed later. The corrector is enabled in all simulations, except in B22 and S42. I have determined the model parameters in Table 6.1 in an iterative trial-and-error manner by assessing the qualitative and quantitative performance of numerous simulations with different parameters. The values for the spatial resolution (n_θ, n_r) represent the resolution at which the error measures have converged or nearly converged to the third digit for a fixed set of parameters.

Figs. 6.1–6.6 are chosen plots for simulation S41, S42 and B21. The measured and simulated bed surface has been extracted along longitudinal or lateral cross-sections at $y = 0$ or $x = 0$, respectively. The dots or crosses denote the nodes of the measured and simulated bed grid. In the measured bed surface, the bottom-piece of the pile appears. The current or waves are traveling from left to right and the arrows refer to bed surfaces of increasing time. Finally, all dimensions in these figures are in meter.

6.1. Error measures

The data set for the error measures are derived in four steps for each measuring time station:

1. The nodes that are defined on the measured bed grid and also reside inside the scour domain are marked.
2. A two-dimensional surface is fitted to the simulated bed elevation. This allows the (fitted) simulated bed surface to be evaluated at the marker nodes that typically do not coincide with the simulated bed grid nodes.
3. Any marker node that falls outside the domain of the fitted simulated bed elevation is omitted from the set of marker nodes. This correction

Table 6.1: Simulations and their parameters. The identifer in 'Exp.' and 'h_0' refers to the set of experimental runs in Hartvig et al. (2010)

Simulation		Development equations								Model physics								Model resolution				
Name	Exp.	V_0/D^3	V_∞/D^3	t_V	ψ_0	ψ_∞	t_ψ	c_1	c_2	h_0	r_{c0}	$r_{\min}$	c_r	μ_s	μ_d	c_p	f_b	$(\Delta h)_{\text{pre,max}}$	$c_{\mu 1}$	$c_{\mu 2}$	n_θ	n_r
		–	–	min	–	–	min	–	–	–	m	m	–	–	–	–	–	m	–	–	–	–
B11	A.02-05	2.5	0.1	113	11	–	–	250	1.9	A.02	0.15	0.05	1.20	0.62	0.51	1.00	1.00	5e-005	1e-003	0.10	360	120
B21	A.08-11	8.0	0.1	113	7.8	–	–	250	1.9	A.08	0.20	0.05	1.20	0.62	0.51	1.00	1.00	5e-005	1e-003	0.10	360	120
B22	A.08-11	8.0	0.1	113	7.8	–	–	250	1.9	A.08	0.20	0.05	1.20	0.62	–	1.00	1.00	5e-005	1e-003	–	360	120
B31	A.14-17	12.9	0.1	113	7.9	–	–	250	1.9	A.14	0.25	0.05	1.20	0.62	0.51	1.00	1.00	5e-005	1e-003	0.10	540	179
B32	A.14-17	12.9	6.8	47	7.9	–	–	1.85e9	8.39	A.14	0.25	0.05	1.20	0.62	0.51	1.00	1.00	5e-005	1e-003	0.10	540	179
S41	A.05-08	0.8	13.7	9.5	160	7.5	0.5	–	–	A.05	0.15	0.05	1.20	0.62	0.51	1.50	1.05	5e-005	1e-003	0.10	360	120
S42	A.05-08	0.8	13.7	9.5	160	7.5	0.5	–	–	A.05	0.15	0.05	1.20	0.62	–	1.50	1.05	5e-005	1e-003	–	360	120
S51	A.11-14	5.8	13.7	9.5	22	7.5	2	–	–	A.11	0.20	0.05	1.50	0.62	0.51	1.50	1.15	5e-005	1e-003	0.10	360	120
S52	A.11-14	5.8	13.3	6.9	22	7.5	1.5	–	–	A.11	0.20	0.05	1.50	0.62	0.51	1.50	1.15	5e-005	1e-003	0.10	360	120

is only relevant when the simulated bed domain does not fully cover the scour domain.

4. The measured bed elevation and fitted simulated bed elevation are evaluated at the marker nodes, leading to the data pair $(h_{\text{meas},j}, h_{\text{sim},j})$, respectively, for the jth of n_j marker nodes.

As error measures, I have chosen the correlation coefficient τ and basic statistics of the error ϵ_j. The correlation coefficient is given as:

$$\tau = \frac{\sum_{j=1}^{n_j} \left(h_{\text{sim},j} - \overline{h_{\text{sim}}}\right) \cdot \left(h_{\text{meas},j} - \overline{h_{\text{meas}}}\right)}{(n_j - 1)\sigma_{h_{\text{meas}}}\sigma_{h_{\text{meas}}}}$$

where τ is the correlation coefficient in the range $[-1, 1]$ where the limits of the range imply perfect correlation. The over-barred quantity $\overline{f}$ and σ_f are the sample mean and sample standard deviation, respectively, of the variable f.

The error is here defined as:

$$\epsilon_j = |h_{\text{sim},j} - h_{\text{meas},j}|, \quad j = 1, 2, \ldots, n_j$$

Based on the array ϵ_j, basic statistical quantities are computed, specifically the *mean* error $\bar{\epsilon}$, the sample *spread* of the error σ_ϵ and the *maximum* error $\epsilon_{\max}$. The error measures for each simulation are shown in Table 6.2 with the error ϵ being normalized to the pile diameter D. The initial simulated bed surface is based on the measured one, but the extracted simulated bed surface at $t = t_m = 0$ has experienced one iteration that involves a corrector and predictor step and therefore deviates slightly from the initial measured one.

6.2. Discussion

The simulated and measured cross-sections agree qualitatively as seen in Figs. 6.1–6.2 and Figs. 6.5–6.6. The error is on average 6% of the pile diameter and at maximum 30% of the pile diameter based on the post-initial bed surfaces ($m = 1, 2, 3$) in Table 6.2. I consider this to be a satisfactory hindcasting performance for the present time when used for soil-structure analyses or design decisions. For other or more specific applications, this assessment may change.

Simulations B31-B32 and S51-52 expose the role of the development equations and the error associated with these. The only difference in input parameters in each of these two pairs of simulation lie in the parameters

Table 6.2: Error measures

Simulation	Time	Error measures				
	t_m	n_j	$\bar{\epsilon}/D$	σ_ϵ/D	$\epsilon_{\max}/D$	τ
	min	–	–	–	–	–
B11	0	304	0.013	0.012	0.054	0.996
	10	304	0.079	0.059	0.260	0.854
	20	304	0.089	0.063	0.245	0.793
	30	304	0.088	0.066	0.286	0.652
B21	0	646	0.010	0.009	0.047	0.999
	10	646	0.030	0.022	0.100	0.990
	20	646	0.042	0.033	0.190	0.972
	30	646	0.061	0.045	0.234	0.944
B22	0	646	0.002	0.001	0.008	1.000
	10	646	0.031	0.023	0.099	0.990
	20	646	0.043	0.033	0.190	0.970
	30	646	0.063	0.046	0.239	0.942
B31	0	909	0.008	0.008	0.040	0.999
	10	909	0.038	0.027	0.115	0.988
	20	909	0.049	0.036	0.188	0.971
	30	909	0.056	0.038	0.182	0.954
B32	0	909	0.008	0.008	0.040	0.999
	10	909	0.037	0.025	0.124	0.989
	20	909	0.048	0.034	0.185	0.972
	30	909	0.056	0.039	0.184	0.954
S41	0	299	0.002	0.003	0.018	0.999
	3	489	0.066	0.047	0.190	0.979
	5	849	0.047	0.036	0.196	0.985
	7	997	0.052	0.042	0.213	0.979
S42	0	299	0.002	0.001	0.009	1.000
	3	488	0.090	0.060	0.301	0.957
	5	849	0.066	0.045	0.228	0.969
	7	997	0.069	0.049	0.283	0.963
S51	0	643	0.003	0.004	0.026	1.000
	3	663	0.089	0.060	0.244	0.962
	13	1364	0.060	0.043	0.234	0.976
	23	1553	0.074	0.055	0.286	0.962
S52	0	643	0.003	0.004	0.026	1.000
	3	741	0.070	0.046	0.183	0.968
	13	1448	0.060	0.041	0.227	0.975
	23	1519	0.074	0.055	0.286	0.961

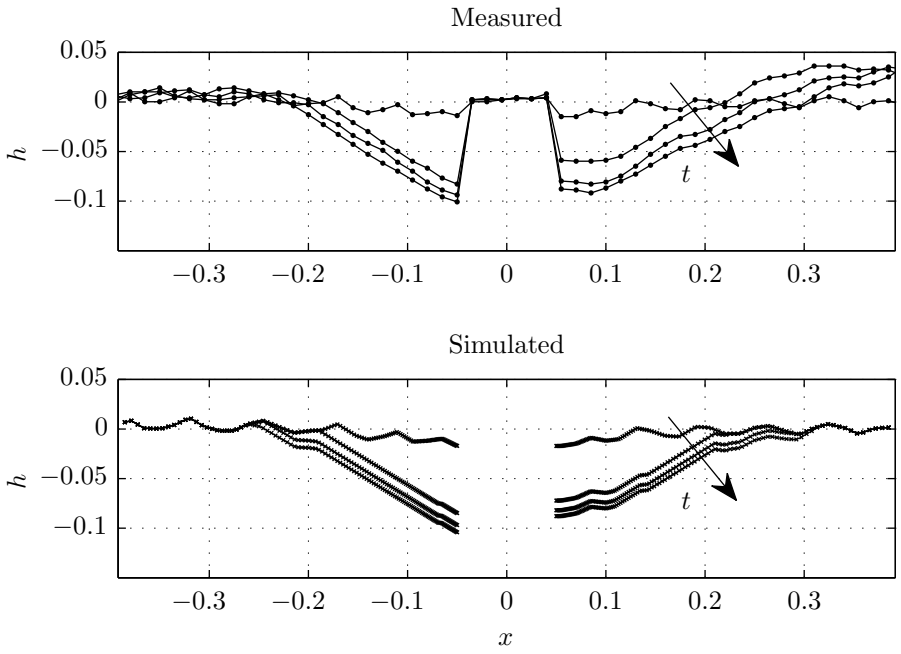

Figure 6.1: Longitudinal sections in scouring simulation S41

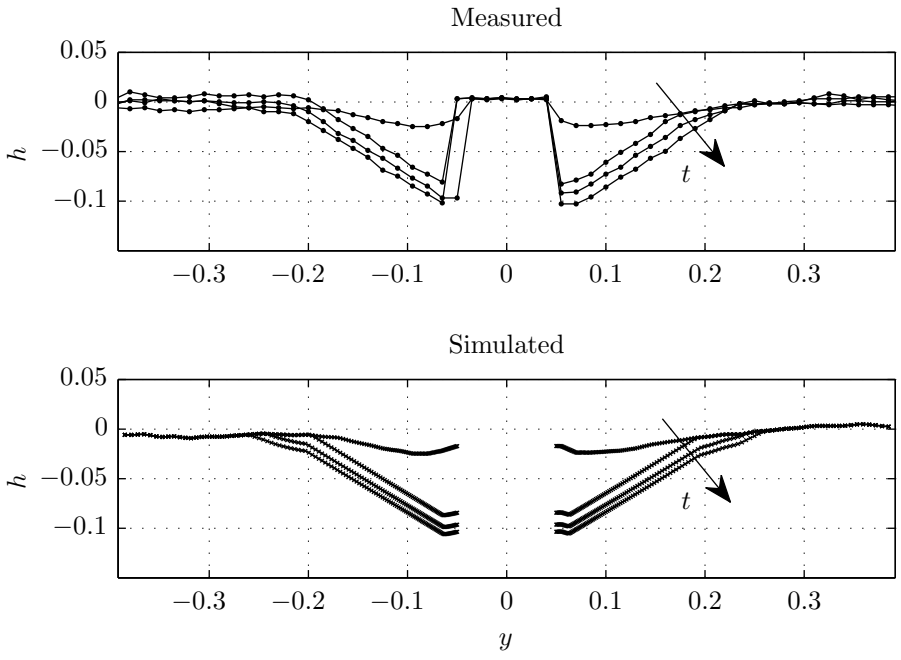

Figure 6.2: Lateral sections in scouring simulation S41

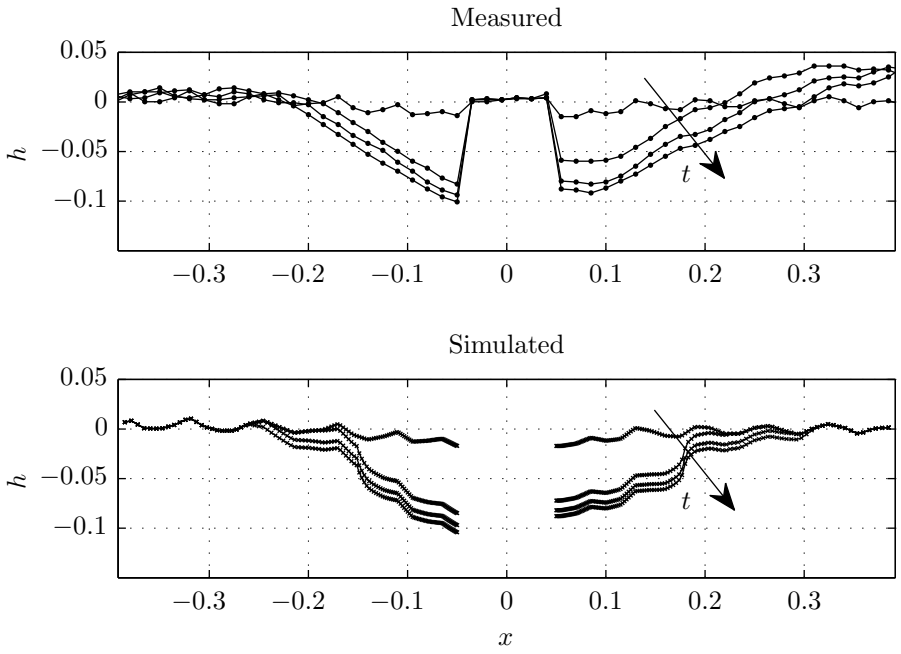

Figure 6.3: Longitudinal sections in scouring simulation S42 (= S41 *without corrector*)

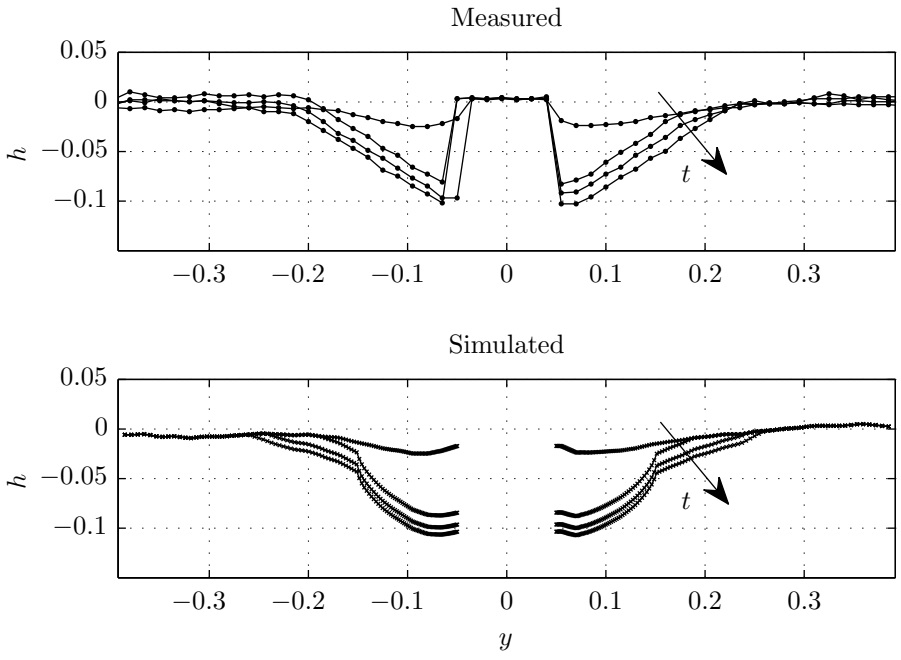

Figure 6.4: Lateral sections in scouring simulation S42 (=S41 *without corrector*)

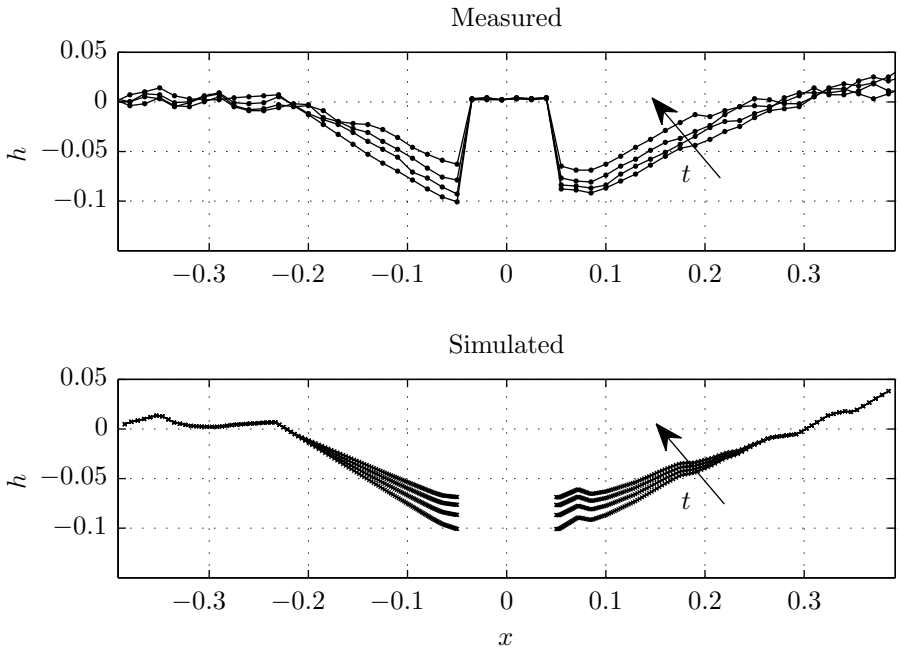

Figure 6.5: Longitudinal sections in backfilling simulation B21

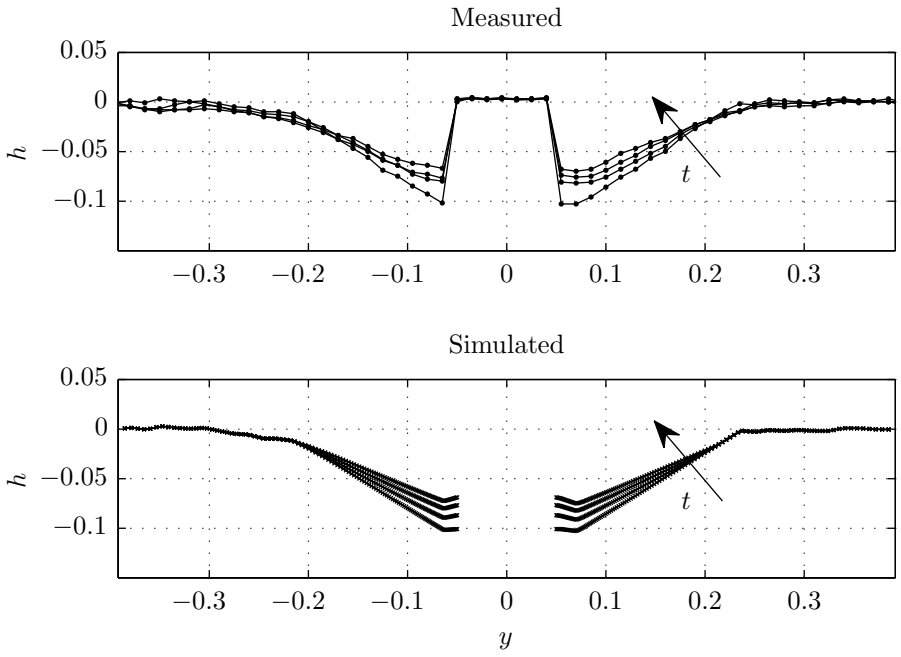

Figure 6.6: Lateral sections in backfilling simulation B21

of the development equations. B32 and S52 use parameters that have been fine-tuned to these respective runs whereas B31 and S51 use parameters that have been fitted to these and the other experimental runs to provide a more general fit. The difference in the mean error relative to the pile diameter is less than 2 percentage points between B31-B32 and S51-S52. This suggests that the hindcasting performance is only slightly improved by fine-tuning the parameters of the development equations in contrast to using the generally-tuned ones.

The role of the corrector is exposed by comparing S41-42 and B21-22 whose input parameters only differ in whether the corrector is enabled or not. During scouring, the simulated and measured bed surfaces agree well qualitatively in S41 in contrast to S42 without the corrector as seen in Fig. 6.1 and Fig. 6.3. The influence of the corrector is much less during backfilling as suggested by the nearly identical error measures of B21 and B22. These results support the hypothesis that sliding plays a leading role during scouring and a minor, perhaps even negligible, role during backfilling. They also support the validity of the components in the corrector.

Turning to the shortcomings of the model, it appears to be less accurate for smaller holes. This can be seen in the error measures where the deviation grows systematically as time increases during the backfilling simulations but remains nearly constant during the scouring simulations. The fundamental cause for this tendency is the general difficulty of dimensioning the smaller holes and characterizing them as a coherent void. For these smaller holes, the concepts of a scour domain and scour volume become less welll-defined, the development equations perform less accurately and the assumption of the coherent distribution of the predictor bed elevation rate becomes cruder. However, I expect that an accurate reproduction of these smaller holes is less critical for typical design purposes. Another shortcoming is the persistence of gentle ripples or downstream banks inside and outside the scour domain in the simulated bed surface that are dissolved in the measured one as seen in Fig. 6.1.

7. Conclusion

In conclusion, I have here presented a model for the bed surface around an offshore monopile. I have aimed at reproducing the geometrical features that appear in the measured bed surfaces of Hartvig et al. (2010) and to accommodate for both scouring and backfilling. The bed elevation rate $\partial h/\partial t$ is distributed in a simple way within the scour domain to fulfill the scour depth rate dS/dt and scour volume rate dS/dt. If the angle of the local

bed slope exceeds the angle of repose, the bed surface is adjusted locally to simulate that these sediment particles slide down the slope until a new equilibrium is achieved.

A comparison between the simulated and measured bed surfaces within the scour domain reveals that they agree qualitatively and that the deviation in bed elevation is on average 6% of the pile diameter and at maximum 30 % of the pile diameter. I consider this to be a satisfactory hindcasting performance for the time being for soil-structure analyses or design decisions. A more comprehensive assessment of the model at the same and more general conditions is encouraged.

Acknowledgment

This study is a part of my PhD study which has been partially funded by Dong Energy Ltd.

References

Subhasish Dey and Abdul Karim Barbhuiya. Time variation of scour at abutments. *J. Hydraulic Eng.*, 131(1):11–23, 2005. ISSN 1943-7900. doi: 10.1061/(ASCE)0733-9429(2005)131:1(11).

Peres Akrawi Hartvig, Jess McCann Thomsen, Peter Frigaard, and Thomas Lykke Andersen. Experimental study of the development of scour & backfilling. *Coastal Eng. J.*, 52(2):157–194, 2010. ISSN 0578-5634. doi: 10.1142/S0578563410002154.

Oscar Link and Ulrich Zanke. On the time-dependent scour-hole volume evolution at a circular pier in uniform coarse sand. In *Proc. 2nd International Conference on Scour and Erosion (ICSE), Singapore*, 2004.

Andreas Roulund. *Three-dimensional numerical modelling of flow around a bottom-mounted pile and its application to scour*. PhD thesis, Technical University of Denmark (DTU), Denmark, 2000.

Andreas Roulund, B. Mutlu Sumer, Jørgen Fredsøe, and Jess Michelsen. Numerical and experimental investigation of flow and scour around a circular pile. *J. Fluid Mechanics*, 534:351–401, 2005. ISSN 0022-1120. doi: 10.1017/S0022112005004507.

B. Mutlu Sumer and Jørgen Fredsøe. *The Mechanics of scour in the marine environment*, volume 17 of *Advances series on Ocean Eng.* World Scientific, 2002. ISBN 981-02-4930-6.

Shinya Umeda, Liang Cheng, Masatoshi Yuhi, and Hajime Ishida. Three-dimensional numerical model of flow and scour around a vertical cylinder. In Jane McKee Smith, editor, *Proc. of 30th Int. Conf. of Coastal Eng.*, volume 3, pages 2354–2366. World Scientific, 2006. doi: 10.1142/9789812709554_0199.

Richard J. S. Whitehouse. *Scour at marine structures: A manual for practical applications*. Thomas Telford Publications, 1998. ISBN 0-7277-2655-2.